Cavity-Enhanced Doppler-Broadening Thermometry via All-Frequency Metrology

Qi Huang (黄琪),[1,*] Jin Wang (王进),[2,†] Rui-Heng Yin (尹睿恒),[1] Yan Tan (谈艳),[1] Cun-Feng Cheng (程存峰),[1,2] Yu R. Sun (孙羽),[3] An-Wen Liu (刘安雯),[4] and Shui-Ming Hu (胡水明)[1,2,4,‡]

[1]*Hefei National Research Center for Physical Sciences at the Microscale, University of Science and Technology of China, Hefei 230026, China*

[2]*Hefei National Laboratory, University of Science and Technology of China, Hefei 230088, China*

[3]*Institute of Advanced Light Source Facilities, Shenzhen 518107, China*

[4]*State Key Laboratory of Chemical Reaction Dynamics, University of Science and Technology of China, Hefei 230026, China*

(Received 14 July 2025; accepted 31 October 2025; published 25 November 2025)

We demonstrate Doppler broadening thermometry (DBT) with all-frequency-domain measurements. Using the R(10) transition of CO at 1567 nm in a high-finesse optical cavity (mode width 0.6 kHz), we resolve Doppler profiles with high signal-to-noise ratios across 2–17 Pa pressures. A global Voigt-profile analysis yields temperatures deviating by only -2.0 ± 3.6 mK from calibrated thermometers, with systematic errors suppressed below 9 ppm. The results show negligible dependence on line-shape models when accounting for pressure effects, resolving a long-standing challenge in DBT. This approach establishes a new paradigm for quantum-based thermometry and provides a precision platform for testing molecular collision physics.

DOI: 10.1103/cy84-v69x

Introduction—The new definition of the kelvin unit [1,2] directly links temperature measurement to the Boltzmann constant k_B. Doppler Broadening Thermometry (DBT) [3–5] has emerged as a prominent high-precision temperature measurement method in recent years due to its unique capability of directly relating thermodynamic temperature to optical frequencies. The relationship between the Doppler width Γ_D (half width at half maximum, HWHM) of atomic or molecular transitions and temperature T can be expressed by the following equation:

$$\frac{\Gamma_D}{\nu_0} = \sqrt{2 \ln 2 \frac{k_B T}{mc^2}} \tag{1}$$

where ν_0 is the central frequency of the transition, T is the thermodynamic temperature, m is the mass of the molecule (atom), and c is the speed of light. Since the first demonstration by Daussy *et al.* [3], DBT studies used various atomic and molecular transitions, such as Rb [6], Cs [7], Hg [8], NH_3 [3,9,10], CO_2 [4,11], C_2H_2 [12–14], and $H_2^{18}O$ [15,16]. The best DBT measurement to date, with an uncertainty of 14 ppm (parts per million), was reported by Gotti *et al.* [11], but with a deviation of about 30 ppm. Castrillo *et al.* demonstrated [14] a DBT result with an uncertainty of 23 ppm and a deviation from the International Temperature Scale of 1990 (ITS-90) of a few millikelvin.

DBT measurements face inherent challenges from non-Doppler broadening mechanisms. While atomic transitions require accounting for the natural linewidth and power broadening effects [17], molecular transitions exhibit complexity due to collision-induced effects, including speed-dependent relaxation and the Dicke effect. The selection of an appropriate line-shape model proves critical for accurate temperature determination [18]. The DBT result reported by Gotti *et al.* [11] employed the complex Hartmann-Tran profile (HTP) [19,20], yet the systematic deviation of such sophisticated models still lacks sufficient experimental verification at the 10^{-6} level [21]. Notably, precise DBT instruments themselves can serve as powerful tools for validating line-shape models at moderate pressures ($10^3 - 10^5$ Pa) close to ambient conditions, with important implications across multiple disciplines including molecular interaction studies [22], atmospheric remote sensing [23,24], and quantum-based gas metrology [25–28].

Experimentally, previous molecular DBT studies using direct absorption spectroscopy exhibited insufficient sensitivity at the low pressures required for minimal collisional effects [4], while cavity ring-down spectroscopy (CRDS) approaches [11,29] were compromised by intensity detection nonlinearities [25,30–32], both potentially introducing systematic line-shape distortions. To address these challenges, we employ cavity mode-dispersion spectroscopy (CMDS) [33–35], a technique combining all-frequency-domain metrology with cavity-enhanced spectroscopy. Frequency measurements offer exceptional accuracy with

*These authors contributed equally to this work.
†Contact author: jinwang@hfnl.cn
‡Contact author: smhu@ustc.edu.cn

minimal interference factors, while cavity enhancement enables high-sensitivity measurements at low gas pressures. This dual strategy permits unprecedented precision in molecular line-shape analysis. As a demonstration, we implement this methodology for high-accuracy DBT measurements, successfully circumventing uncertainties associated with collisional broadening.

Experimental—The experiment employed CMDS to measure Doppler-broadened absorption spectra in the near-infrared. As illustrated in Fig. 1(a), the setup was adapted from established methodologies reported in Refs. [27,36]. The system mainly consisted of a 118-cm linear optical cavity with high-reflectivity mirrors ($R = 99.997\%$) operating in the $1.5 - 1.7$ μm spectral range, yielding a free spectral range (FSR) of 126.9 MHz and a mode linewidth of 0.6 kHz. An external-cavity diode laser (ECDL) served as the light source, with its output split into "locking" and "probing" beams. The locking beam was stabilized to a cavity mode via Pound-Drever-Hall (PDH) frequency locking. The probing beam was sequentially modulated through an acousto-optic modulator (AOM) and a fiber-coupled electro-optic modulator (EOM) before being injected into the cavity. The radio-frequency system was synchronized using a GPS-disciplined rubidium clock (SRS FS725), enabling frequency scanning via dynamic EOM rf switching. Transmission signals were detected when AOM-EOM synthesized frequency shifts matched cavity mode frequencies.

As illustrated in Fig. 1(b), the optical cavity was enclosed in a stainless-steel vacuum chamber, with coarse temperature regulation provided by external heating tapes. A dual-layer aluminum alloy cylinder system was implemented between the vacuum chamber and optical cavity: the outer layer incorporated a servo-locked active temperature control system using resistive heating wire, achieving submillikelvin stability, while the inner layer acted as a thermal shield.

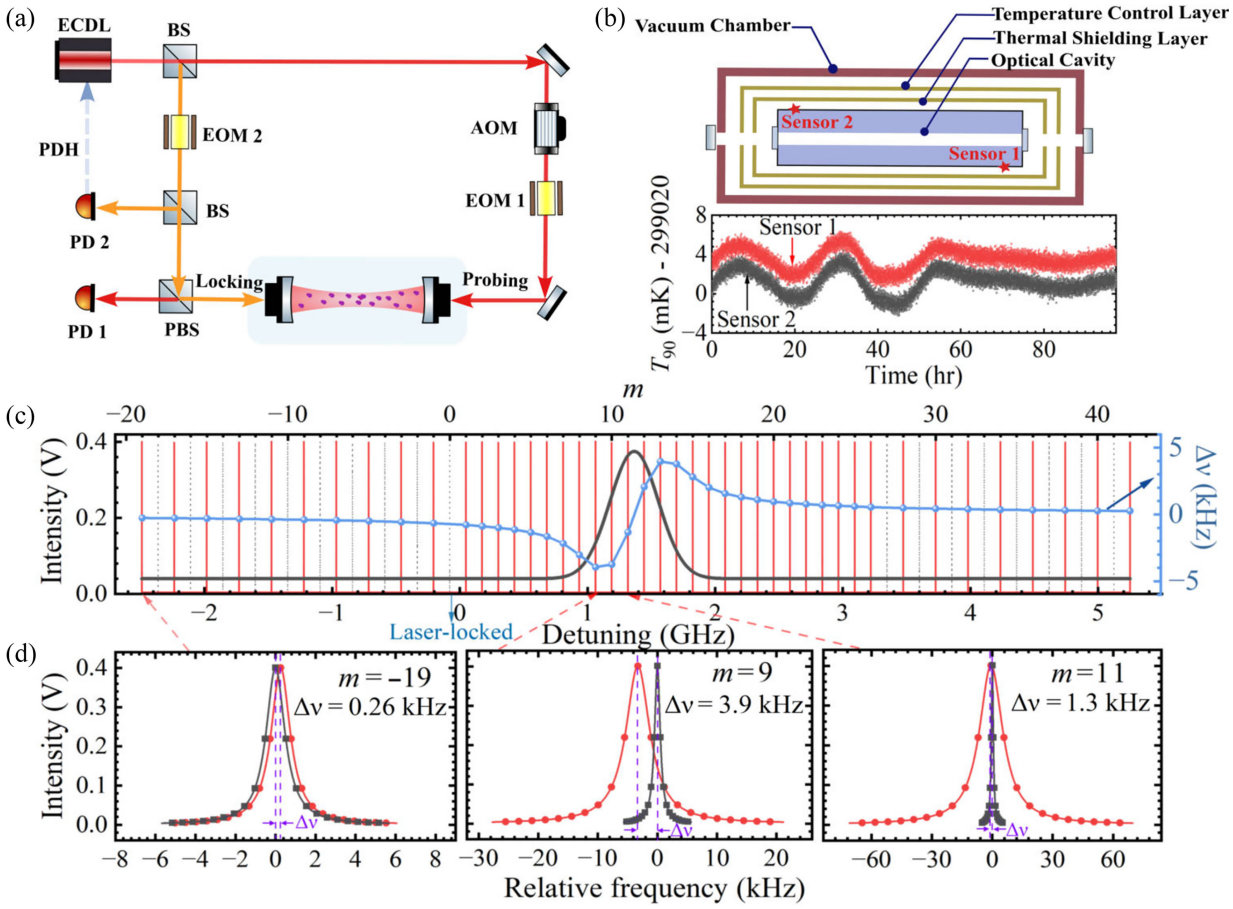

FIG. 1. (a) Configuration of the experimental setup. Abbreviations: AOM, acousto-optic modulator; BS, beam splitter; ECDL, external-cavity diode laser; EOM, electro-optic modulator; PBS, polarizing beam splitter; PD, photodiodes. (b) Structure of the sample cell and optical cavity. Temperatures were measured by two standard platinum resistance thermometers (SPRTs) placed on both sides of the inner aluminum cavity. (c) The experimental dispersion spectrum (blue dots) and the simulated absorption spectrum (black line) of CO (9.58 Pa). The locking beam was locked at the $m = 0$ mode of the cavity via PDH locking. The probing beam measured the frequency centers of modes with m in the range of -19 to 42, indicated by red vertical lines. (d) Transmitted spectra of three cavity modes with indexes of $m = -19$, 9, and 11, are given in the lowest panel. Red dots and black squares represent signals recorded with and without CO gas. Note that profiles (black curves) are almost identical for all the modes of an empty cavity.

The temperature of the inner aluminum shield was monitored by two standard platinum resistance thermometers (SPRTs) placed on both sides [see Fig. 1(b)]. These sensors were connected to an MKT50 readout, and the readings have been calibrated at the National Institute of Metrology (Beijing, China) with 1 mK accuracy. As shown in Fig. 1(b), a continuous four-day operation near 299 K demonstrated temperature fluctuations within ±2 mK and the difference between the two SPRTs readings was about 2 mK, confirming excellent thermal stability and spatial uniformity.

In CMDS measurements, a 8-GHz spectral scan range was implemented with sampling across over 40 cavity modes, as shown in Fig. 1(c). Transmittance spectra around a given cavity mode were recorded to determine the mode center frequency. A few samples of the cavity mode spectra are shown in the figure. For each mode, the difference $\Delta\nu$ between the resonance frequencies with and without gas was measured, yielding the dispersion spectrum. This spectrum is intrinsically linked to the conventional absorption spectrum through the Kramers-Krönig relations. To speed up scanning, some modes far from the absorption peak were skipped in the measurement. This approach achieved single-spectrum acquisition in about 6 s.

Selecting an appropriate molecular transition is critical for DBT measurements. After evaluating line lists of various molecules in the infrared region, we selected the R(10) line of the (3-0) band of $^{12}C^{16}O$, located at 6385.77 cm^{-1}. The calculated Doppler width (HWHM) at the experimental temperature of 299.022 K is 224.0630 MHz. The line position has been determined with kilohertz accuracy [37], and the line strength was measured [26] to be 1.9491×10^{-23} cm molecule^{-1} at 296 K with a fractional uncertainty of 0.1%. Prior measurements [13] confirmed that nearby lines from minor CO isotopologues contribute negligibly at the 10^{-6} level, making this transition ideal for high-precision spectroscopy.

The CO sample pressure in this Letter ranged from 2 to 17 Pa, corresponding to an absorption coefficient of 6×10^{-7} to 5×10^{-6} cm^{-1} at the center. This ensured both sufficient SNR and minimal collision-induced broadening. Gas samples with a stated purity of 99.99% were used, and liquid-nitrogen cold traps were employed to remove impurities such as water vapor. The CO pressure was validated using the integrated absorbance (I_A) of the recorded spectrum and the line strength $S(T)$: $P = I_A k_B T / S(T)$. Figure 2(a) shows dispersion spectra of the R(10) line recorded at three different pressures.

DBT temperature—The profile of the CMDS spectrum can be described as follows [27,33]:

$$\frac{\Delta\nu}{\nu_m} = I_A \times \frac{\mathrm{Im}\left[\varphi(\nu_m - \nu_c)\right]}{2nk_0} \tag{2}$$

where ν_m is the frequency of the cavity mode with index of m; n is the frequency-independent refractive index of the gas; k_0 is the wave vector of the transition frequency; and $\Delta\nu$ is the frequency shift of the cavity mode due to the dispersion induced by the molecular absorption line. The line shape of the dispersion spectra is the imaginary part of the normalized line-shape function $\varphi(\nu_m - \nu_c)$.

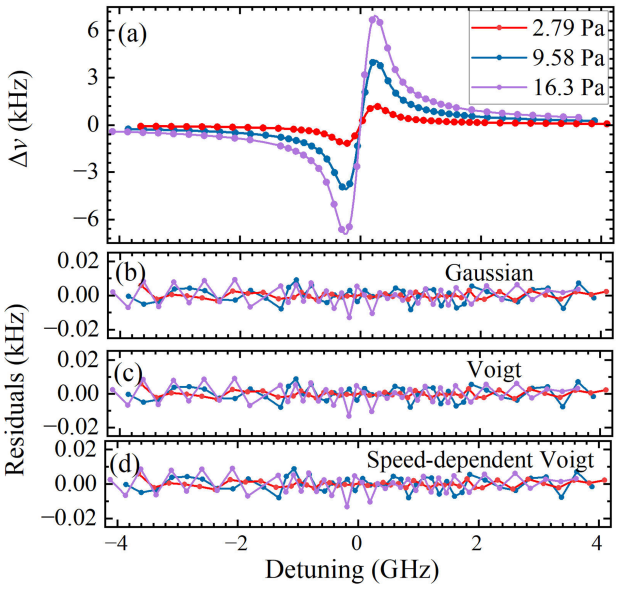

FIG. 2. (a) Dispersion spectra of the R(10) (3-0) line of CO, single scan, pressures at 2.79, 9.58, and 16.3 Pa. Experimental data (single scan) in scattering points and fitted spectra in solid lines. Residuals of fitting with Gaussian, Voigt, and speed-dependent Voigt profiles are shown in panels (b)–(d).

The Voigt profile was used in spectra fitting, accounting for the Gaussian Doppler broadening and the Lorentzian collisional broadening. A global fitting procedure was applied to fit all spectra recorded under different pressures. The Gaussian half-width was set to be identical for all spectra recorded under the same temperature and treated as a free parameter. The Lorentzian half-width was set proportional to the gas pressure (P):

$$\Gamma_L = \gamma_0 P, \tag{3}$$

where γ_0 is the collision-induced broadening coefficient. For each spectrum, the amplitude, center position, and a linear baseline were set free in the global fitting. Eventually, we obtained a coefficient of $\gamma_0 = 18.52(19)$ kHz/Pa from the global fitting, which agrees reasonably with the value 18.98 kHz/Pa at 299 K given in Ref. [38] and 18.64 kHz/Pa @296 K given in the HITRAN database [39]. Note that the collision broadening coefficient exhibits a temperature dependence. Within a narrow temperature range such as 296–300 K, the resulting variation in the self-broadening coefficient [40,41] is less than 1%. We also attempted to fit the spectra with Gaussian and speed-dependent Voigt (SDV) profiles, with the latter extending the Voigt model by considering molecular velocity

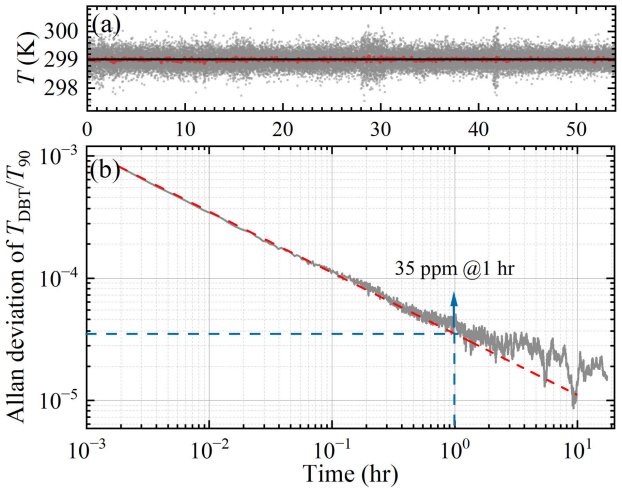

FIG. 3. DBT compared with thermal sensor, Allan deviation (a) DBT temperatures (T_{DBT}, gray circles) and T_{90} (black line) from SPRT sensors. The red line indicates the averaged T_{DBT} results of every 50 spectra. (b) Allan deviation of the ratios T_{DBT}/T_{90}.

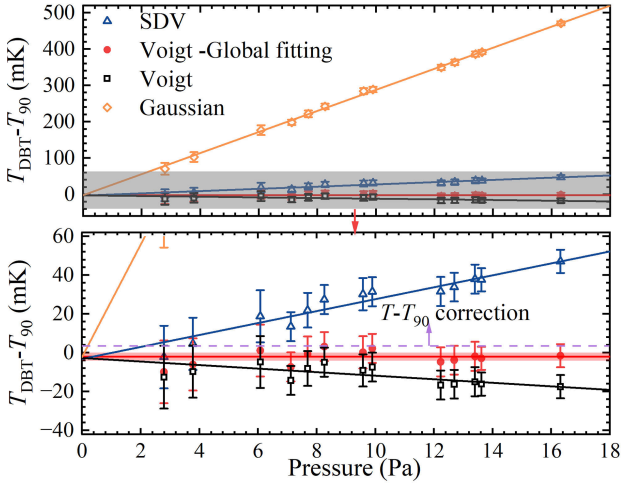

FIG. 4. Comparison of the DBT temperatures T_{DBT} and readings from thermal sensors (T_{90}). T_{DBT} values at different pressures were derived using different line profiles: speed-dependent Voigt (parameters from Ref. [38]; blue triangles), Voigt from global fitting in this Letter (red dots), Voigt with HITRAN [39] parameters (black squares), and Gaussian (orange diamonds). The purple dashed line indicates the difference between the T_{90} value and the thermodynamic temperature at 299.0 K. The red line and belt indicate the mean value (−2.0 mK) and standard deviation (2.2 mK) of the results from the Voigt-Global Fit model. See main text for details.

distribution effects. Fitting residuals are shown in the lower panels of Fig. 2. We can see that no considerable difference can be observed. Note that the collision-induced broadening of CO is only one-sixth that of NH_3, due to ammonia's much larger dipole moment [42]. The high-order collision-induced effects become less significant at such low pressures. Therefore, the Voigt profile was applied in this Letter.

Using the collision broadening coefficient of $\gamma_0 = 18.52$ kHz/Pa, we refit each spectrum to determine the DBT temperature. Figure 3(a) shows the DBT temperatures (gray dots) obtained in 55 h at a pressure of 9.58 Pa, alongside the thermosensor temperature readings (black line). The red line represents average values of every 50 DBT temperatures taken in approximately six-minute intervals. Figure 3(b) displays the Allan deviation of the ratio between the DBT temperature and the sensor temperature. The Allan deviation decreases at a rate of 2100 ppm $Hz^{-1/2}$ with increasing averaging time, reaching approximately 35 ppm after 1 h.

Figure 4 presents the DBT temperatures measured at various pressures (red dots). As expected, higher pressures improve the signal-to-noise ratio (SNR) of the spectra, reducing the statistical uncertainty in the derived DBT temperatures. After correcting for pressure-induced broadening, the statistical uncertainty in the DBT temperature is 2.2 mK (7 ppm), with a mean deviation of −2.0 mK compared to the reference platinum resistance thermometer readings (T_{90}). The NIM-calibrated SPRT sensors have an uncertainty of 1 mK, while the temperature gradient across the sample cell was maintained below 2 mK. For comparison, the purple dashed line in the figure indicates the $T - T_{90}$ correction of 3.5 mK proposed in Ref. [43].

Systematic uncertainties—The choice of line profile model in DBT measurements critically determines both precision and accuracy [5]. Benefiting from the high sensitivity of cavity-enhanced spectroscopy and the low gas pressure employed in this Letter (2–17 Pa), pressure broadening was smaller than Doppler broadening by 3–4 orders of magnitude, allowing the Voigt profile to accurately reproduce the experimental spectra. As previously mentioned, we fixed the pressure broadening coefficient to the value obtained from global fitting and then determined the Gaussian broadening through fitting. The weighted mean DBT temperature is -2.0 ± 2.2 mK deviating from the T_{90} value. For comparison, we also performed spectral fitting using the broadening coefficients recommended in the HITRAN database. The resulting Gaussian broadening values, shown as black squares in Fig. 4, exhibit a noticeable pressure dependence. By performing linear extrapolation to zero pressure, we obtained a DBT temperature with a -3.1 ± 3.3 mK deviation from T_{90}. Furthermore, we employed Gaussian and SDV profiles to fit the experimental spectra, with coefficients γ_0 and γ_2 in the SDV model fixed to values reported in Ref. [38]. The obtained Gaussian half-widths at different pressures are indicated in Fig. 4. Linear extrapolation to zero pressure yielded a DBT temperature with -2.1 ± 3.9 mK (Gaussian) and -2.6 ± 3.2 mK (SDV) deviated from T_{90}, again in agreement with the global fitting result. These comparisons demonstrate that the result is insensitive

to the choice of line-shape model. Even when potential deviations exist in the line-shape model or its parameters, consistent DBT temperatures can be obtained after pressure extrapolation. The maximum discrepancy (1.1 mK) between these different line-shape approaches serves as our estimate of the systematic uncertainty introduced by the line-shape model in DBT measurements.

Other contributions to the uncertainty budget include collision broadening due to water vapor emitted during the measurement (6 ppm); saturation effect (4 ppm); gas pressure measurement (1 ppm); temperature gradient along the optical cavity (3 ppm); and frequency calibration and laser linewidth (< 1 ppm). Details of these contributions are given in the End Matter. The total systematic (type-B) uncertainty is 9 ppm. Together with the statistical (type-A) uncertainty of 7 ppm, the overall uncertainty is 12 ppm. We also experimentally investigated the influence of potential error sources on DBT temperature measurements via measurements under different conditions. As shown in the End Matter, most of the deviations are consistent with the 12-ppm uncertainty.

Conclusion—Our all-frequency-based DBT measurements yield a temperature that deviates by -2.0 ± 3.6 mK from the readings of platinum resistance thermometers. The result comprises 7 ppm statistical and 9 ppm systematic uncertainties. This represents the most precise DBT measurement achieved to date. The consistency of results across varying pressure conditions confirms the method's effectiveness in eliminating systematic biases from collisional effects. The remaining systematic error likely stems from gas desorption in the vacuum chamber—an effect that could be significantly mitigated in future implementations. Further improvements in laser locking stability could enhance the signal-to-noise ratio, thereby reducing statistical uncertainties. It should be noted that the reference SPRT itself has an uncertainty of 1 mK and requires a 3.5 mK correction to account for the difference between the thermodynamic temperature and ITS-90 [43,44]. A theoretical or precise experimental determination of the temperature-dependent pressure-broadening effect [40,41] would enable the application of this method across a wide temperature range, making it a valuable tool for validating differences between ITS-90 and thermodynamic temperature.

Beyond its immediate application in temperature measurement at low pressures, our platform enables high-precision investigations of collisional effects, such as non-Markovian dynamics [22], at elevated pressures. By providing rigorous validation for molecular collision models, it addresses a critical need in atmospheric remote sensing, where accurate line-shape predictions are essential [23]. Furthermore, this Letter paves the way for a quantum-based foundation in gas metrology [25,28,45] and creates opportunities to develop high-accuracy spectroscopic standards with versatile applications.

Acknowledgments—This work was jointly supported by the Independent Deployment Project of HFNL (Grant No. ZB2025010500), the Strategic Priority Research Program of the Chinese Academy of Sciences (Grants No. XDB0970100, No. XDA0520304), the Innovation Program for Quantum Science and Technology (Grants No. 2021ZD0303102, No. 2023ZD0301000), and the National Natural Science Foundation of China (Grants No. 12393825, No. 22241302).

Data availability—The data that support the findings of this article are openly available [46].

[1] J. Fischer *et al.*, The Boltzmann project, Metrologia **55**, R1 (2018).
[2] M. Stock, R. Davis, E. de Mirandés, and M. J. T. Milton, The revision of the SI—The result of three decades of progress in metrology, Metrologia **56**, 022001 (2019).
[3] C. Daussy, M. Guinet, A. Amy-Klein, K. Djerroud, Y. Hermier, S. Briaudeau, Ch. J. Bordé, and C. Chardonnet, Direct determination of the Boltzmann constant by an optical method, Phys. Rev. Lett. **98**, 250801 (2007).
[4] G. Casa, A. Castrillo, G. Galzerano, R. Wehr, A. Merlone, D. Di Serafino, P. Laporta, and L. Gianfrani, Primary gas thermometry by means of laser-absorption spectroscopy: Determination of the Boltzmann constant, Phys. Rev. Lett. **100**, 200801 (2008).
[5] R. Gotti, M. Lamperti, D. Gatti, and M. Marangoni, Laser-based primary thermometry: A review, J. Phys. Chem. Ref. Data **50**, 031501 (2021).
[6] G.-W. Truong, E. F. May, T. M. Stace, and A. N. Luiten, Quantitative atomic spectroscopy for primary thermometry, Phys. Rev. A **83**, 033805 (2011).
[7] G. W. Truong, J. D. Anstie, E. F. May, T. M. Stace, and A. N. Luiten, Accurate lineshape spectroscopy and the Boltzmann constant, Nat. Commun. **6**, 8345 (2015).
[8] S. Gravina, N. A. Chishti, A. Castrillo, L. Gianfrani, A. Sorgi, P. C. Pastor, C. Clivati, F. Bertiglia, G. Lopardo, F. Levi, and G. Galzerano, Comb-locked deep-ultraviolet laser system for precision mercury spectroscopy, Phys. Rev. A **109**, 022816 (2024).
[9] K. Djerroud, C. Lemarchand, A. Gauguet, C. Daussy, S. Briaudeau, B. Darquié, O. Lopez, A. Amy-Klein, C. Chardonnet, and C. J. Bordé, Measurement of the Boltzmann constant by the Doppler broadening technique at a 3.8×10^{-5} accuracy level, C. R. Phys. **10**, 883 (2009).
[10] C. Lemarchand, M. Triki, B. Darquié, C. H. Bordé, C. Chardonnet, and C. Daussy, Progress towards an accurate determination of the Boltzmann constant by Doppler spectroscopy, New J. Phys. **13**, 073028 (2011).
[11] R. Gotti, L. Moretti, D. Gatti, A. Castrillo, G. Galzerano, P. Laporta, L. Gianfrani, and M. Marangoni, Cavity-ring-down Doppler-broadening primary thermometry, Phys. Rev. A **97**, 012512 (2018).
[12] K. M. T. Yamada, A. Onae, F.-L. Hong, H. Inaba, and T. Shimizu, Precise determination of the Doppler width of a rovibrational absorption line using a comb-locked diode laser, C. R. Phys. **10**, 907 (2009).

[13] C. F. Cheng, J. Wang, Y. R. Sun, Y. Tan, P. Kang, and S. M. Hu, Doppler broadening thermometry based on cavity ring-down spectroscopy, Metrologia **52**, S385 (2015).
[14] A. Castrillo, E. Fasci, H. Dinesan, S. Gravina, L. Moretti, and L. Gianfrani, Optical determination of thermodynamic temperatures from a C_2H_2 line-doublet in the near infrared, Phys. Rev. Appl. **11**, 064060 (2019).
[15] L. Moretti, A. Castrillo, E. Fasci, M. D. De Vizia, G. Casa, G. Galzerano, A. Merlone, P. Laporta, and L. Gianfrani, Determination of the Boltzmann constant by means of precision measurements of $H_2{}^{18}O$ line shapes at 1.39 μm, Phys. Rev. Lett. **111**, 060803 (2013).
[16] E. Fasci, M. D. De Vizia, A. Merlone, L. Moretti, A. Castrillo, and L. Gianfrani, The Boltzmann constant from the $H_2{}^{18}O$ vibration-rotation spectrum: Complementary tests and revised uncertainty budget, Metrologia **52**, S233 (2015).
[17] G. W. Truong, D. Stuart, J. D. Anstie, E. F. May, T. M. Stace, and A. N. Luiten, Atomic spectroscopy for primary thermometry, Metrologia **52**, S324 (2015).
[18] L. Gianfrani, Linking the thermodynamic temperature to an optical frequency: Recent advances in Doppler broadening thermometry, Phil. Trans. R. Soc. A **374**, 20150047 (2016).
[19] N. Ngo, D. Lisak, H. Tran, and J.-M. Hartmann, An isolated line-shape model to go beyond the Voigt profile in spectroscopic databases and radiative transfer codes, J. Quant. Spectrosc. Radiat. Transfer **129**, 89 (2013).
[20] J. Tennyson *et al.*, Recommended isolated-line profile for representing high-resolution spectroscopic transitions (IUPAC technical report), Pure Appl. Chem. **86**, 1931 (2014).
[21] J. M. Hartmann, H. Tran, R. Armante, C. Boulet, A. Campargue, F. Forget, L. Gianfrani, I. Gordon, S. Guerlet, M. Gustafsson, J. T. Hodges, S. Kassi, D. Lisak, F. Thibault, and G. C. Toon, Recent advances in collisional effects on spectra of molecular gases and their practical consequences, J. Quant. Spectrosc. Radiat. Transfer **213**, 178 (2018).
[22] Z. D. Reed, H. Tran, H. N. Ngo, J.-M. Hartmann, and J. T. Hodges, Effect of non-Markovian collisions on measured integrated line shapes of CO, Phys. Rev. Lett. **130**, 143001 (2023).
[23] D. J. Jacob, D. J. Varon, D. H. Cusworth, P. E. Dennison, C. Frankenberg, R. Gautam, L. Guanter, J. Kelley, J. McKeever, L. E. Ott, B. Poulter, Z. Qu, A. K. Thorpe, J. R. Worden, and R. M. Duren, Quantifying methane emissions from the global scale down to point sources using satellite observations of atmospheric methane, Atmos. Chem. Phys. **22**, 9617 (2022).
[24] H. Tran, J. V. Auwera, T. Bertin, W. Fakhardji, O. Pirali, and J.-M. Hartmann, Absorption of methane broadened by carbon dioxide in the 3.3 μm spectral region: From line centers to the far wings, Icarus **384**, 115093 (2022).
[25] A. J. Fleisher, E. M. Adkins, Z. D. Reed, H. Yi, D. A. Long, H. M. Fleurbaey, and J. T. Hodges, Twenty-five-fold reduction in measurement uncertainty for a molecular line intensity, Phys. Rev. Lett. **123**, 043001 (2019).
[26] K. Bielska, A. A. Kyuberis, Z. D. Reed, G. Li, A. Cygan, R. Ciuryło, E. M. Adkins, L. Lodi, N. F. Zobov, V. Ebert, D. Lisak, J. T. Hodges, J. Tennyson, and O. L. Polyansky, Subpromille measurements and calculations of CO (3-0) overtone line intensities, Phys. Rev. Lett. **129**, 043002 (2022).
[27] Q. Huang, Y. Tan, R.-H. Yin, Z.-L. Nie, J. Wang, and S.-M. Hu, Line intensities of CO near 1560 nm measured with absorption and dispersion spectroscopy, Metrologia **61**, 065003 (2024).
[28] J. T. Hodges, K. Bielska, M. Birk, R. Guo, G. Li, J. S. Lim, D. Lisak, Z. D. Reed, and G. Wagner, International comparison CCQM-P229 pilot study to measure line intensities of selected $^{12}C^{16}O$ transitions, Metrologia **62**, 08006 (2025).
[29] Y. R. Sun, H. Pan, C.-F. Cheng, A.-W. Liu, J.-T. Zhang, and S.-M. Hu, Application of cavity ring-down spectroscopy to the Boltzmann constant determination, Opt. Express **19**, 19993 (2011).
[30] A. Cygan, S. Wójtewicz, M. Zaborowski, P. Wcisło, R. Guo, R. Ciuryło, and D. Lisak, One-dimensional cavity mode-dispersion spectroscopy for validation of CRDS technique, Meas. Sci. Technol. **27**, 045501 (2016).
[31] S. Wójtewicz, D. Lisak, A. Cygan, J. Domysławska, R. S. Trawiński, and R. Ciuryło, Line-shape study of self-broadened O_2 transitions measured by Pound-Drever-Hall-locked frequency-stabilized cavity ring-down spectroscopy, Phys. Rev. A **84**, 032511 (2011).
[32] A. Cygan, S. Wójtewicz, H. Jóźwiak, G. Kowzan, N. Stolarczyk, K. Bielska, P. Wcisło, R. Ciuryło, and D. Lisak, Dispersive heterodyne cavity ring-down spectroscopy exploiting eigenmode frequencies for high-fidelity measurements, Sci. Adv. **11**, 8556 (2025).
[33] A. Cygan, P. Wcisło, S. Wójtewicz, P. Masłowski, J. T. Hodges, R. Ciuryło, and D. Lisak, One-dimensional frequency-based spectroscopy, Opt. Express **23**, 14472 (2015).
[34] P. Kang, Y. Sun, J. Wang, L. An-Wen, and S.-M. Hu, Measurement of molecular absorption spectrum with a laser locked on a high-finesse cavity, Acta Phys. Sin. **67**, 104206 (2018).
[35] A. Cygan, P. Wcisło, S. Wójtewicz, G. Kowzan, M. Zaborowski, D. Charczun, K. Bielska, R. S. Trawiński, R. Ciuryło, P. Masłowski, and D. Lisak, High-accuracy and wide dynamic range frequency-based dispersion spectroscopy in an optical cavity, Opt. Express **27**, 21810 (2019).
[36] L.-G. Tao, A.-W. Liu, K. Pachucki, J. Komasa, Y. R. Sun, J. Wang, and S.-M. Hu, Toward a determination of the proton-electron mass ratio from the Lamb-dip measurement of HD, Phys. Rev. Lett. **120**, 153001 (2018).
[37] J. Wang, C.-L. Hu, A.-W. Liu, Y. Sun, Y. Tan, and S.-M. Hu, Saturated absorption spectroscopy near 1.57 μm and revised rotational line list of $^{12}C^{16}O$, J. Quant. Spectrosc. Radiat. Transfer **270**, 107717 (2021).
[38] Q. Huang, J. Wang, J.-K. Li, Z.-L. Nie, A.-W. Liu, Y. Tan, and S.-M. Hu, Line shape parameters of self-broadened CO transitions in the (3-0) overtone band, J. Quant. Spectrosc. Radiat. Transfer **343**, 109483 (2025).
[39] I. Gordon *et al.*, The HITRAN2020 molecular spectroscopic database, J. Quant. Spectrosc. Radiat. Transfer **277**, 107949 (2022).
[40] V. Malathy Devi, D. Chris Benner, M. Smith, A. Mantz, K. Sung, L. Brown, and A. Predoi-Cross, Spectral line parameters including temperature dependences of self- and

air-broadening in the 2-0 band of CO at 2.3 μm, J. Quant. Spectrosc. Radiat. Transfer **113**, 1013 (2012).
[41] R. Hashemi, I. E. Gordon, E. M. Adkins, J. T. Hodges, D. A. Long, M. Birk, J. Loos, C. D. Boone, A. J. Fleisher, A. Predoi-Cross, and L. S. Rothman, Improvement of the spectroscopic parameters of the air- and self-broadened N_2O and CO lines for the HITRAN2020 database applications, J. Quant. Spectrosc. Radiat. Transfer **271**, 107735 (2021).
[42] M. Triki, C. Lemarchand, B. Darquié, P. L. T. Sow, V. Roncin, C. Chardonnet, and C. Daussy, Speed-dependent effects in NH_3 self-broadened spectra: Towards the determination of the Boltzmann constant, Phys. Rev. A **85**, 062510 (2012).
[43] J. Fischer, M. de Podesta, K. D. Hill, M. Moldover, L. Pitre, R. Rusby, P. Steur, O. Tamura, R. White, and L. Wolber, Present estimates of the differences between thermodynamic temperatures and the ITS-90, Int. J. Thermophys. **32**, 12 (2011).
[44] C. Gaiser, B. Fellmuth, R. M. Gavioso, M. Kalemci, V. Kytin, T. Nakano, A. Pokhodun, P. M. C. Rourke, R. Rusby, F. Sparasci, P. P. M. Steur, W. L. Tew, R. Underwood, R. White, I. Yang, and J. Zhang, 2022 update for the differences between thermodynamic temperature and ITS-90 below 335 K, J. Phys. Chem. Ref. Data **51**, 043105 (2022).
[45] G. Li, A. Röttger, M. Zboril, and O. Werhahn, Metrology for climate action, Measurement **38**, 101850 (2025).
[46] Q. Huang, J. Wang, R.-H. Yin, Y. Tan, C.-F. Cheng, Y. R. Sun, A.-W. Liu, and S.-M. Hu, Data in "Cavity-enhanced Doppler-broadening thermometry via all-frequency metrology", Mendeley Data, 2025, 10.17632/6p2fykmk5w.1.
[47] J. Wang, Y. R. Sun, L.-G. Tao, A.-W. Liu, and S.-M. Hu, Communication: Molecular near-infrared transitions determined with sub-kHz accuracy, J. Chem. Phys. **147**, 091103 (2017).
[48] Y. Tan, T.-P. Hua, J.-D. Tang, J. Wang, A.-W. Liu, Y. R. Sun, C.-F. Cheng, and S.-M. Hu, Self- and N_2—broadening of CO in the low-pressure regime, J. Phys. Conf. Ser. **2439**, 012007 (2023).

End Matter

The purity of the CO sample gas is 99.99%. Before entering the cavity, potential gas impurities such as water vapor were removed using a liquid nitrogen cold trap. However, gas desorption from the inner walls of the cavity and vacuum pipelines can induce systematic deviations due to collision broadening of the CO transition. The primary influence here comes from the desorption of water vapor inside the cavity. In the experiment, the release of water vapor was monitored using a nearby absorption line of the water molecule. The results show that, over several hours of measurement, the water vapor pressure remained below 0.03 Pa. Based on the collision broadening coefficient of 31.3 kHz/Pa for water molecules affecting the CO R(10) line, as provided by the HITRAN database [39], we estimate that the impact of this effect on DBT measurements is less than 6 ppm.

Saturation effects in an intense laser field lead to spectral line broadening. In this Letter, the homogeneous broadening of the CO line is dominated by transit-time broadening and collision broadening. The Lamb dip width of 0.1 MHz measured in our previous experiments [37,47,48] corresponds to a saturation power of about 4.3 W. At a circulating intracavity power of 0.2 W, the saturation parameter is approximately 0.046, corresponding to an additional broadening of 0.8 kHz. The resulting deviation to the DBT temperature is 4 ppm.

The uncertainty in the pressure P of the CO gas used is about 0.1%. According to the correction given by Eq. (3), when DBT measurements are conducted below 10 Pa, the contribution of the pressure P precision to the uncertainty in the linewidth is approximately 0.2 kHz, and its contribution to the uncertainty in the DBT temperature measurement is below 1 ppm.

There was a ± 1 mK temperature gradient of the sample cell, corresponding to an uncertainty of 3 ppm.

The laser was locked to a longitudinal mode of an ultrahigh-finesse optical cavity with a mode linewidth of approximately 0.6 kHz. All radio frequencies were synchronized to a GPS-disciplined rubidium clock (SRS FS725). Since the laser linewidth was even much narrower than the width of cavity modes, its impact on the DBT measurement was well below 1 ppm.

An uncertainty budget is given in Table I. Including the statistical uncertainty (7 ppm) and the systematic uncertainty due to the line profile model (4 ppm) discussed in the main text, the overall uncertainty is 12 ppm.

We systematically evaluated the influence of potential error sources on DBT temperature measurements through experimental investigations. The results are presented in

TABLE I. Error budget ($k = 1$) of AF-DBT.

Type	Source	u_r/ppm
A	Statistical	7
B	Line-shape model	4
	Gas desorption	6
	Saturation effect	4
	Pressure	1
	Temperature gradient	3
	Frequency scale and laser linewidth	<1
Total		12

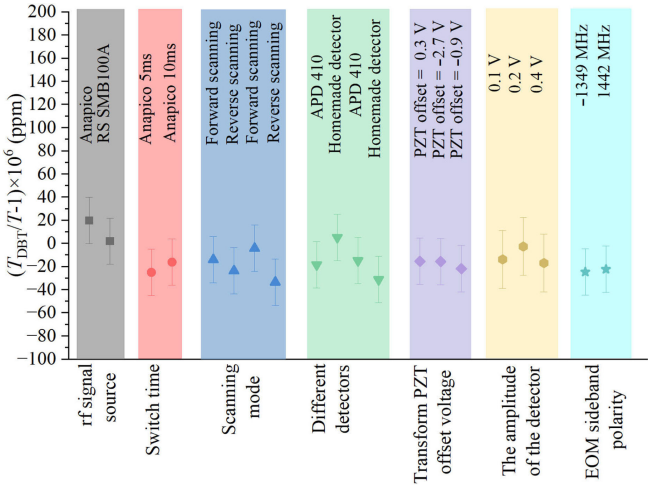

FIG. 5. Consistency check of AF-DBT measurements.

Fig. 5 with the horizontal axis representing various error sources and the vertical axis showing the deviation between DBT temperature and the platinum thermal sensor temperature.

Radio frequency source: A comparison between the Rohde and Schwarz SMB100A and the AnaPico Apusyn20 signal sources measured at 9.58 Pa (gray box) revealed that their deviations were within the experimental error range. Subsequent experiments employed the Apusyn20 rf source.

Radio frequency switching time: Tests at 13.6 Pa comparing 5 ms and 10 ms switching durations showed no considerable deviation. Thus, 5 ms switching was adopted to enhance efficiency.

Scanning mode: Alternating tests between forward and reverse scans at 12.7 Pa demonstrated no statistically significant difference. Therefore, an alternating scanning mode was implemented.

Detector: Comparative tests (four repeated measurements) between two detectors, Thorlabs APD410 and a custom-built detector, confirmed good agreement. The APD410 exhibited better stability and was consequently selected for subsequent measurements.

PZT locking: Tests with different locking servo bias voltages of 0.3, 0.9, and 2.7 V showed no significant impact on the results.

Laser power: Measurements with signal peak heights of 0.1, 0.2, and 0.4 V indicated negligible variations, so the peak height was fixed at 0.4 V for subsequent experiments.

EOM sideband polarity: Scans using both positive and negative sidebands yielded negligible deviations, and the positive sideband mode was adopted.